Energy Proceedings
Vol 43, 2024
ISSN 2004-2965

Towards a 24/7 Carbon-Free Electric Fleet: A Digital Twin Framework

Mateus Gheorghe de Castro Ribeiro[1*], Justin Luke[1*], Sonia Martin[2], Emmanuel Balogun[2], Gustavo Vianna Cezar[3], Marco Pavone[4], Ram Rajagopal[1]

1 Department of Civil and Environmental Engineering, Stanford University, Stanford, CA, USA

2 Department of Mechanical Engineering, Stanford University, Stanford, CA, USA

3 Applied Energy Division, SLAC National Accelerator Laboratory, Menlo Park, CA, USA

4 Department of Aeronautics and Astronautics, Stanford University, Stanford, CA, USA
(*Authors have equal contributions. Corresponding Authors: {mateusgh, jthluke}@stanford.edu)

ABSTRACT

This paper proposes a 24/7 Carbon-Free Electric Fleet digital twin framework for modeling, controlling, and analyzing an electric bus fleet, co-located solar photovoltaic arrays, and a battery energy storage system. The framework consists of forecasting modules for marginal grid emissions factors, solar generation, and bus energy consumption that are input to the optimization module, which determines bus and battery operations at minimal electricity and emissions costs. We present a digital platform based on this framework. For a case study of Stanford University's Marguerite Shuttle, the platform reduced peak charging demand by 99%, electric utility bill by $2779, and associated carbon emissions by 100% for one week of simulated operations for 38 buses. When accounting for operational uncertainty, the platform still reduced the utility bill by $784 and emissions by 63%.

Keywords: decarbonization, electric buses, digital twin, charging scheduling, battery storage, optimal planning

1. INTRODUCTION

In 2022, energy production and transportation contributed to more than 50% of natural gas and petroleum usage in the United States [1]. According to the United Nations, fossil fuels are the leading contributors to global climate change, representing more than 75% of greenhouse gas emissions and close to 90% of all carbon dioxide emissions [2]. Thus, ensuring clean electricity generation and transportation is crucial to eliminating greenhouse gas emissions.

Vehicle electrification is a viable means of reducing emissions. Studies project there will be more than 300 million light-duty electric vehicles (EVs) worldwide in 2035 [3]. For medium- and heavy-duty vehicles, ordinances like the 2018 Innovative Clean Transit Regulation require that all California public transit agency fleets be zero-emission by 2040 [4].

To efficiently meet the emissions reduction target and mitigate global warming, electricity demand from EV fleet charging must come from non-fossil fuel sources. Currently, a battery EV charging on the US grid's most carbon-intensive power mix produces 30% more emissions than a hybrid counterpart [5]. Therefore, monitoring the grid for times of lower carbon emissions is necessary to maximize the use of cleaner energy when coordinating EV charging.

However, coordinating charging for medium and heavy-duty EV fleets while respecting their schedule constraints is challenging. Many papers concentrate on charging coordination to reduce costs [6, 7]. Others focus on bus fleet operation and charging management [8]. The daily cost of charging and deadhead driving was minimized with a mixed-integer linear program (MILP) model in a city case study with available solar and wind energy sources. Similar works also adopt a MILP model for coordinating EV fleets and respective charging schedules and locations [9, 10, 11, 12].

Several works have also used other techniques, such as random search with particle swarm optimization and a polynomial time algorithm in a real-world case study [13]. Other works explore using a Markov decision process to minimize electricity usage and cost [14] and nonlinear programming to minimize electricity cost and battery aging [15].

Many of these electric bus fleet charging and operation coordination works, however, do not account

This is a paper for 15th International Conference on Applied Energy (ICAE2023), Dec. 3-7, 2023, Doha, Qatar.

for emissions, the addition of co-located storage, or electricity demand charges [16]. The methods in [17] and [18] minimize emissions but do not jointly optimize for electricity costs, vehicle operations, or integration of battery storage. In [17], compared to the baseline, results demonstrated that the method could reduce 26% of carbon emissions, still far from a fully decarbonized bus fleet.

1.1 Contributions

To the best of the authors' knowledge, no other study has proposed a platform that simultaneously accounts for emissions and costs in the route assignment, charge scheduling, battery storage dispatch, and photovoltaic (PV) solar coordination joint problem. Thus, the main contributions of this work are as follows:

- A digital twin framework composed of forecast modules and an optimization module to coordinate PV solar, storage, and routes and charging schedules of an electric bus fleet system.
- A demonstration of the proposed approach in a real-world context using real data from the Stanford Marguerite Shuttle transit system.
- Forecasting models that predict PV solar generation and marginal emissions factors, and a surrogate model that estimates bus energy consumption while accounting for variability in factors.
- An optimization module that solves a MILP to determine bus-run and charging assignments and battery storage dispatching while minimizing electricity and carbon emissions costs.

An overview of the digital twin is shown in Fig. 1, summarizing the various modules, input features that are predicted or known, and platform outputs. We demonstrate the application of the 24/7 Carbon-Free Electric Fleet (CFEF) Platform for the Stanford Marguerite Shuttle in different scenarios with varying times of year, solar generation capacities, inclusion of battery storage. We then compare these simulated optimal results with the actual Marguerite Shuttle charging profiles and costs in 2023.

1.2 Paper Organization

The remainder of the paper is organized as follows. Section 2 presents the forecasting, surrogate, and optimization models that constitute the 24/7 CFEF Platform. Section 3 describes the case study which demonstrates the platform. Section 4 presents the results and their main takeaways. Finally, Section 5 summarizes conclusions and suggests future work.

2. PROBLEM SETUP

2.1 Forecasting

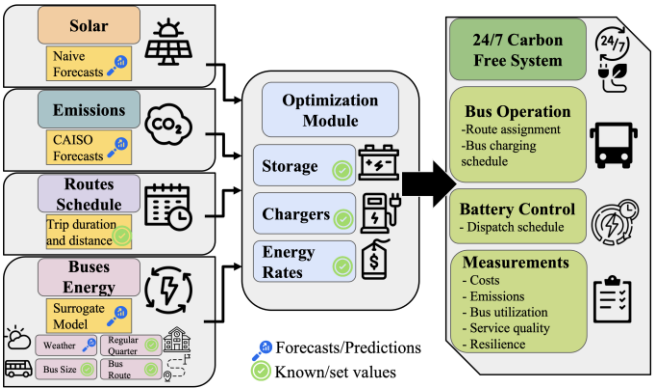

Fig. 1. Schematic of Digital Twin Framework.

We use simple forecast modules for PV solar and marginal grid emissions factors, which are input to the optimization module. For solar, we used a seasonal moving average where the next day forecast is the average of the last three days. For emissions, we use the marginal emissions forecasts provided by the California Independent System Operator (CAISO) Self-Generation Incentive Program API[1]. As CAISO API forecasts up to three days only, values from the same day of week of the previous week are used to forecast emissions beyond three days. Lastly, we also forecast weather, which is input to the surrogate model that predicts bus energy consumption. We use a daily moving average of the last two days. We evaluate forecast accuracy with Weighted Mean Absolute Percentage Error ($WMAPE$).

2.2 Surrogate Model

Many factors influence the energy consumption of a bus, including driver behavior, battery aging, weather (which can affect HVAC usage and battery performance), bus occupancy, and route taken. To predict uncertain energy consumption, we use a Gaussian Process-based surrogate model, which is a probabilistic model that allows us to infer a distribution over data points based on known input-output values [19, 20].

We assume that the output y, bus energy consumption average for a given route in a given day, is mapped by a function $f(\boldsymbol{x})$ added with noise $\epsilon \sim \mathcal{N}(0, \sigma^2)$. The vector $\boldsymbol{x}$ comprises a set of features that account for uncertainty in bus energy consumption, including bus size (large or small), route

[1] https://content.sgipsignal.com/api-documentation

taken, weather variables, and whether the day is a regular school day. The weather variables are obtained via the Stanford Western Weather group[2] and include daily max, min, and average temperature (°F); daily rain (in); daily solar radiation (cal/cm^2); Heating Degree Days ($HDDs$) and Cooling Degree Days ($CDDs$).

A set of known $\boldsymbol{x}$, $X = \{\boldsymbol{x}^{(1)}, \boldsymbol{x}^{(2)}, \dots, \boldsymbol{x}^{(m)}\}$ associated to the respective set of bus energy average consumption $\boldsymbol{y} = y^{(1)}, y^{(2)}, \dots, y^{(m)}\}$ can be used to predict the values of unmapped energy consumption, $\hat{\boldsymbol{y}}$, from a set of unmapped X^* [19, 20]. The training dataset comprises of the last 30 days, while the next seven days are used to test the trained surrogate model using metrics like the Mean Squared Error (MSE) and Coefficient of Determination (R^2).

2.3 Optimization

The optimization module of the 24/7 CFEF Platform determines bus-run assignments, bus charging, and battery storage charging/discharging at minimum cost, which includes electric utility energy and demand charges, revenue from power injected back to the grid, and carbon emissions cost. We model this optimization problem as a MILP, described in Eq. (17), with decision variables listed in Table 1. Fig. 2 shows the key power flow decision variables and their relationship with the system components. The problem is solved for a horizon consisting of a set of equidistant time steps, $\mathcal{T}$, of duration Δ_t in hours, for a set of heterogeneous buses $\mathcal{B}$, and for operating a set of bus runs $\mathcal{R}$.

Decision Variable	Domain	Description
y^{batt}_{charge}	$\{0,1\}^{\lvert\mathcal{T}\rvert}$	Indicator for battery charging
$y^{batt}_{discharge}$	$\{0,1\}^{\lvert\mathcal{T}\rvert}$	Indicator for battery discharging
SoC^{batt}	$\mathbb{R}^{\lvert\mathcal{T}\rvert}_{\geq 0}$	State of charge of battery
P^{batt}_{solar}	$\mathbb{R}^{\lvert\mathcal{T}\rvert}_{\geq 0}$	Power from solar to battery
P^{batt}	$\mathbb{R}^{\lvert\mathcal{T}\rvert}$	Battery power
$P^{batt}_{charger}$	$\mathbb{R}^{\lvert\mathcal{T}\rvert}_{\geq 0}$	Power discharged from battery to charger
$P^{batt}_{grid,charger}$	$\mathbb{R}^{\lvert\mathcal{T}\rvert}_{\geq 0}$	Power from grid to charge battery
$P^{batt}_{grid,discharge}$	$\mathbb{R}^{\lvert\mathcal{T}\rvert}_{\geq 0}$	Power discharged from battery to grid
$P^{charger}$	$\mathbb{R}^{\lvert\mathcal{T}\rvert}_{\geq 0}$	Charger power
$P^{charger}_{grid}$	$\mathbb{R}^{\lvert\mathcal{T}\rvert}_{\geq 0}$	Power from grid to charger
$P^{charger}_{solar}$	$\mathbb{R}^{\lvert\mathcal{T}\rvert}_{\geq 0}$	Power from solar to charger
$[y^b]_{b\in\mathcal{B}}$	$\{0,1\}^{\lvert\mathcal{T}\rvert}$	Indicator for charging for bus b
$[SoC^b]_{b\in\mathcal{B}}$	$\mathbb{R}^{\lvert\mathcal{T}\rvert}_{\geq 0}$	State of charge of bus b
$[P^b]_{b\in\mathcal{B}}$	$\mathbb{R}^{\lvert\mathcal{T}\rvert}$	Power of bus b
$[P^b_{charge}]_{b\in\mathcal{B}}$	$\mathbb{R}^{\lvert\mathcal{T}\rvert}_{\geq 0}$	Charging power of bus b
$[x_s]_{s\in\mathcal{S}}$	$\{0,1\}^{\lvert\mathcal{B}_s\rvert\times\lvert\mathcal{R}_s\rvert}$	Assignment matrix for buses and runs of type s
P^{grid}_{max}	$\mathbb{R}^{n_{demand\ charge}}_{\geq 0}$	Maximum power from grid
P^{solar}_{grid}	$\mathbb{R}^{\lvert\mathcal{T}\rvert}_{\geq 0}$	Power from solar to grid
SoC^{batt}_{init}	$\mathbb{R}_{\geq 0}$	Initial state of charge of battery
$[SoC^b_{init}]_{b\in\mathcal{B}}$	$\mathbb{R}_{\geq 0}$	Initial state of bus b

Table 1: Decision variables used in the optimization model. All power variables are in units of kW. SoC^{batt}_{init} and $[SoC^b_{init}]_{b\in\mathcal{B}}$ can also be fixed inputs.

[2] https://stanford.westernweathergroup.com/

The following equations model the stationary battery storage for the system:

$$SoC^{batt}[1] = SoC^{batt}_{init} \tag{1}$$

$$SoC^{batt}[1] = SoC^{batt}[|\mathcal{T}|] \tag{2}$$

$$SoC^{batt}[t] \geq SoC^{batt}_{min}\ \forall t \in \mathcal{T} \tag{3}$$

$$SoC^{batt}[t] \leq SoC^{batt}_{max}\ \forall t \in \mathcal{T} \tag{4}$$

$$P^{batt}[t] = \eta_{batt}\left(P^{batt}_{grid,charge}[t] + P^{batt}_{solar}[t]\right) - \frac{1}{\eta_{batt}}\left(P^{batt}_{grid,discharge}[t] + P^{batt}_{charger}[t]\right)\ \forall t \in \mathcal{T} \tag{5}$$

$$SoC^{batt}[t] = SoC^{batt}[t-1] + \frac{P^{batt}[t]\Delta_t}{E_{batt}}\quad \forall t \in \{2,\dots,|\mathcal{T}|\} \tag{6}$$

$$P^{batt}_{grid,charge}[t] + P^{batt}_{solar}[t] \leq y^{batt}_{charge}[t]\overline{P}^{batt}\ \forall t \in \mathcal{T} \tag{7}$$

$$P^{batt}_{grid,discharge}[t] + P^{batt}_{charger}[t] \leq y^{batt}_{discharge}[t]\underline{P}^{batt}\quad \forall t \in \mathcal{T} \tag{8}$$

$$y^{batt}_{charge}[t] + y^{batt}_{discharge}[t] \leq 1\ \forall t \in \mathcal{T} \tag{9}$$

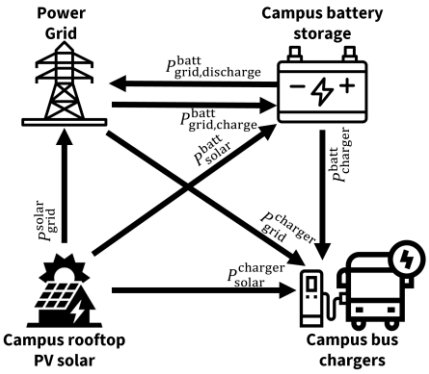

Fig. 2. Schematic of power flow as modeled in the optmization problem.

Eq. (1) sets the battery state of charge (SoC) at the first time step to $SoC^{batt}_{init} \in [0,1]$, which can be a fixed input or a decision variable. Eq. (2) is the periodicity constraint setting the SoC at the last time step equal to that of the first time step. Eq. (3) and Eq. (4) bound the SoC to maintain a desired backup power reserve or mitigate battery degradation. Eq. (5) defines the power flow within the battery, where η_{batt} is the battery's charging and discharging efficiency. Eq. (6) defines the SoC evolution, where E_{batt} is the battery's rated energy capacity in kWh. Eq. (7) and Eq. (8) bounds the battery charging and discharging power, where $\overline{P}^{batt}$ and $\underline{P}^{batt}$ are the rated charging and discharging rate limits of the battery, respectively. Eq. (9) is the complementarity constraint that ensures the battery cannot simultaneously charge and discharge. The battery model assumes it can charge or discharge up to its rated power at any SoC.

Buses can park or charge at the bus depot, where the chargers and on-site PV solar are located, and where they begin and end each run. Each bus is

characterized by a type $s \in \mathcal{S}$, comprised of varying size, energy consumption, charging speed, and battery capacity. Each run $r \in \mathcal{R}$ has a specified start and end time in $\mathcal{T}$ and a specified type $s \in \mathcal{S}$ for the type of buses that serve r. The following equations model each bus $b \in \mathcal{B}$:

$$SoC^b[1] = SoC^b_{init} \tag{10}$$

$$SoC^b[1] = SoC^b[|\mathcal{T}|] \tag{11}$$

$$SoC^b[t] \geq SoC^b_{min} \; \forall t \in \mathcal{T} \tag{12}$$

$$SoC^b[t] \leq SoC^b_{max} \; \forall t \in \mathcal{T} \tag{13}$$

$$P^b_{charge}[t] \leq \eta_{charger}\eta_b min\left(\overline{P}^b, \overline{P}^{charger}\right) \quad \forall b \in \mathcal{B}, \forall t \in \mathcal{T} \tag{14}$$

$$P^b[t] = P^b_{charge}[t] - \sum_{r \in \mathcal{R}_{s,t}} x_s[b,r]\, E_{r,s} \quad \forall b \in \mathcal{B}, \forall t \in \mathcal{T}, \forall s \in \mathcal{S} \tag{15}$$

$$SoC^b[t] = SoC^b[t-1] + \frac{P^b[t]\Delta_t}{E_b} \; \forall t \in \{2, \ldots, |\mathcal{T}|\} \tag{16}$$

Eq. (10) sets the initial SoC of bus b. Eq. (11) is the periodicity constraint. Eq. (12) and Eq. (13) bound the bus' SoC, used for leaving a bus battery reserve to buffer against operational uncertainties or to mitigate bus battery degradation. Eq. (14) upper bounds the charging power of the bus, where $\eta_{charger}$ is the charging supply equipment's efficiency, η_b is the bus battery's charging efficiency, $\overline{P}^b$ is the bus' maximum charging (and discharging) rate, and $\overline{P}^{charger}$ is the charger's maximum charging rate. Eq. (15) determines the power flow within the bus' battery, where $E_{r,s}$ is the energy consumed in kWh by a bus of type s completing run r, and $\mathcal{R}_{s,t}$ is the subset of runs with buses of type s and are in service at time t. Eq. (16) defines the SoC evolution, where E_{batt} is the bus battery's rated energy capacity in kWh. This bus model assumes a constant charging curve (charge power is not limited by SoC) and that the chargers and buses are capable of throttling the charging power.

Finally, the optimization problem Eq. (17) combines the above battery storage and bus modeling equations with other system decision variables and constraints and a cost minimization objective function:

$$\min_{Table\ 1} \sum_{t \in \mathcal{T}} \Delta_t \left(P^{charger}_{grid}[t] + P^{batt}_{grid,charge}[t]\right) \cdot \left(p_{CO_2} CO_2^{grid}[t] + p_{energy}[t]\right) \tag{17a}$$

$$+ \sum_{i=1}^{n_{demand\,charge}} P^{grid}_{max}[i] p_{demand}[i] \tag{17b}$$

$$- \sum_{t \in \mathcal{T}} \Delta_t \left(P^{batt}_{grid,discharge}[t] + P^{solar}_{grid}[t]\right) \cdot p_{energy,revenue}[t] \tag{17c}$$

$$-\lambda\left(SoC^{batt}[1] + \sum_{b \in \mathcal{B}} SoC^b[1]\right) \tag{17d}$$

subject to

Stationary Battery constraints, Eqs. (1) – (9)

Bus constraints $\forall b \in \mathcal{B}$, Eqs. (10) – (16)

$$\sum_{b \in \mathcal{B}_s} x_s^{b,r} = 1 \quad \forall r \in \mathcal{R}_s, \forall s \in \mathcal{S} \tag{17e}$$

$$\sum_{r \in \mathcal{R}_{s,\text{overlap},i}} x_s^{b,r} \leq 1 \quad \forall b \in \mathcal{B}_s \tag{17f}$$

$$\forall \mathcal{R}_{s,\text{overlap},i} \in \left(\mathcal{R}_{s,\text{overlap},i}\right)_{i \in I}, \forall s \in \mathcal{S}$$

$$\sum_{r \in \mathcal{R}_{s,t}} x_s^{b,r} + y^b[t] \leq 1 \quad \forall b \in \mathcal{B}_s, \forall t \in \mathcal{T}, \forall s \in \mathcal{S} \tag{17g}$$

$$\sum_{b \in \mathcal{B}} y^b[t] \leq n_{charger} \quad \forall t \in \mathcal{T} \tag{17h}$$

$$P^{charger}[t] = P^{charger}_{grid}[t] + P^{charger}_{solar}[t] + P^{batt}_{charger}[t] \quad \forall t \in \mathcal{T} \tag{17i}$$

$$P^{charger}[t] = \sum_{b \in \mathcal{B}} \frac{P^b_{charge}[t]}{\eta_{charger}\eta_b}, \forall t \in \mathcal{T} \tag{17j}$$

$$P^{solar}_{grid}[t] = P^{solar}[t] - P^{batt}_{solar}[t] - P^{charger}_{solar}[t] \; \forall t \in \mathcal{T} \tag{17k}$$

$$P^{grid}[t] \leq P^{grid}_{max}[i] \quad \forall i \in \{1, \ldots, |n_{demand\ charge}|\}, \forall t \in \mathcal{T}_{demand\ charge\ i} \tag{17l}$$

$$\frac{\sum_{b \in \mathcal{B}} SoC^b[t] E_b}{\sum_{b \in \mathcal{B}} E_b} \geq SoC^{fleet}_{min} \; \forall t \in \mathcal{T} \tag{17m}$$

In the objective function, the first term, Eq. (17a), includes the electric energy charges and carbon emissions cost. The energy consumed at time t from the grid loads, the battery storage and the chargers, is multiplied by the sum of the time-of-use energy price $p_{energy}[t]$ $(\$/kWh)$ and the per-energy carbon price, which is the product of carbon price, $p_{CO_2}[t]$ $(\$/tCO_2)$ and marginal grid emissions factor, $CO_2^{grid}[t]$ (tCO_2/kWh). The second term, Eq. (17b), is the sum of the $n_{demand\,charge}$ demand charges, for which each demand charge i is the product of the maximum power during that demand charge and its price, $p_{demand}[i]$ $(\$/kW)$. The third term, Eq. (17c), is the revenue or cost offset obtained by injecting power back into the grid at an energy price of $p_{energy,revenue}$ $(\$/kWh)$. Lastly, the fourth term, Eq. (17d), is a small reward, weighted by λ, that allows the optimization problem to favor solutions with higher battery and bus initial SoC to allow for greater operational flexibility, with negligible impact to the total objective. This term only has an effect when SoC^{batt}_{init} and SoC^b_{init} $\forall b \in \mathcal{B}$ are decision variables. As this term is not actual revenue, it is subtracted from the optimal objective in post-optimization.

In the constraints, Eq. (17e) enforces that among the subset of buses of type s, $\mathcal{B}_s$, exactly one bus is assigned to run r. This is repeated for all runs of type s, denoted by $\mathcal{R}_s$, and for all types $s \in \mathcal{S}$. Eq. (17f) enforces that a bus b of type s can only serve at most one run at a given time, where I indexes all subsets $\mathcal{R}_{s,overlap,i}$ of runs of type s that collectively share at least one time step of overlap. Eq. (17g) enforces that a

bus b cannot both serve a run and charge at a given time t. Eq. (17h) upper bounds the number of buses that can charge at time t by the number of charger plugs, $n_{charger}$. Eq. (17i) defines the supply of charger power, which can come from the grid, PV solar, or battery storage. Eq. (17j) defines the demand of charger power, which is the sum of the charging power of the buses after accounting for losses. Eq. (17k) defines the surplus PV solar generated. Because $P_{grid}^{solar} \in \mathbb{R}_{\geq 0}$, the battery storage and the chargers are constrained to not exceed the available solar generation. Eq. (17l) defines the maximum power during each demand charge period i, where $\mathcal{T}_{demand\ charge,i}$ is the set of time steps in demand charge period i. Finally, Eq. (17m) lower bounds the fleet-wide average SoC to SoC_{min}^{fleet}, weighted by each bus' battery capacity. When $SoC_{min}^{b} < SoC_{min}^{fleet}$, this constraint ensures not all buses are near its minimum charge limit simultaneously.

The optimization model in Eq. (17) can be used for real-time operation with model predictive control. Specifically, $P^{solar}[t]$, $CO_2^{grid}[t]$, and $E_{r,s}\ \forall r \in \mathcal{R}, \forall s \in \mathcal{S}$ are prediction inputs from the solar forecasting module, emissions forecasting module, and the surrogate model of the bus energy consumption, respectively. SoC_{init}^{batt} and $SoC_{init}^{b}\ \forall b \in \mathcal{B}$ define the system's initial state which can be updated from the current battery storage and bus state of charge measurements.

3. CASE STUDY

Based on the digital twin framework presented in Section 2, we develop a platform in Python for simulating optimal electric bus fleet operations for a case study of Stanford University's Marguerite Shuttle[3], which serves approximately 15 publicly-open routes on and off campus and has an annual ridership of over 2.74 million. To develop the digital twin, we used data from (i) bus telemetry, which includes average energy consumption for each route and bus of a given size, (ii) generation profiles of the PV solar array located at the Marguerite bus depot, (iii) CAISO marginal grid emissions factors, (iv) weather-related features, and (v) Stanford academic calendar data.

The Marguerite fleet has three bus models, BYD models K7, K9, and K9M, with battery capacity E_b of $180kWh$, $324kWh$, and $313kWh$, respectively. K7 buses are type "small" whereas K9 and K9M buses are type "large" and all have a charging efficiency of $\eta_b = 0.9$. When not serving a route, the buses are located at a single bus depot with parking spaces and $n_{charger} = 24$ chargers rated at $\bar{P}^{charger} = 80kW$ AC with an efficiency of $\eta_{charger} = 0.95$; from data, charging power is observed to be constant regardless of SoC. Each Marguerite route is divided into scheduled runs assigned to specific buses. A run begins at the bus depot, completes a specified number of loops of a given route, and ends at the bus depot. This study considers 38 Stanford-operated electric buses with routes divided into 255 runs per week in January and March and 261 runs in May. A fleet average minimum SoC of $SoC_{min}^{fleet} = 0.5$ is used.

A $1.8MW$ array of rooftop PV solar panels located at the bus depot provide carbon-free energy to the charging stations. The solar system is not exclusively used for bus charging; university facilities use any surplus electricity generation. Thus, the price of energy revenue, $p_{energy,revenue}$, for power injected back to the grid from solar surplus or battery storage discharging is assumed to be equal to the price for energy consumption, p_{energy}, in this case study. Fig. 3 (left) depicts the average solar profile for January, March, and May 2023. The amount of solar varies considerably across seasons, with a peak close to $700kW$ during the winter to a peak of almost double in May with approximately $1300kW$.

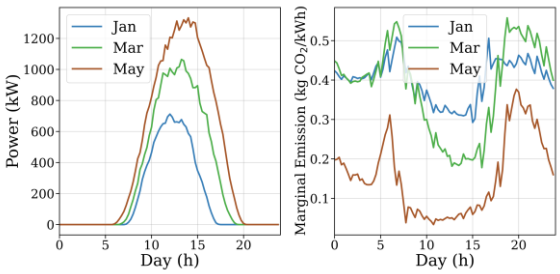

Fig. 3. For January, March, and May 2023, daily average generation profile for the PV solar array at Stanford's bus depot (left) and CAISO marginal emissions factors (right)

As described in Section 2.1, this work uses historical marginal emissions factors from CAISO to forecast future grid emissions. We set the p_{CO_2}, to equal a social cost of carbon of \$180 per tCO_2 [21]. Fig. 3 (right) depicts the average marginal emissions. Notice how in the winter and beginning of Spring, when fewer renewable resources are available, the marginal emissions factors are considerably higher with values between 0.2 and 0.5 $kg \cdot CO_2/kWh$. In May, there are daylight hours when the marginal emissions factors average is lower than 0.05 $kg \cdot CO_2/kWh$.

[3] https://transportation.stanford.edu/marguerite

The price of electricity, particularly demand charges, is a key element when determining cost-minimizing operations. Stanford uses the PG&E E-20 Transmission Firm tariff (see Table 2), which is divided into energy charges, the price of energy consumed every 15 minutes ($\$/kWh$), and $n_{demand\ charge} = 3$ demand charges, determined by the largest power peak in 15 minutes during specified periods of the monthly billing period ($\$/kW$). In this study, some scenarios include a storage system to be installed at the Stanford bus depot. It has a capacity of $E_{batt} = 752kWh$, a maximum charge/discharge rate of $\overline{P}^{batt} = 300\ kW$ efficiency of $\eta_{batt} = 0.95$, and $SoC_{min}^{batt} = 0.2$.

Energy Charges		
Rate	**Period**	**($\$/kWh$)**
Peak Summer	12:00pm-6:00 pm	0.12337
Part-Peak Summer	8:30am-6:00pm and 6pm-9:30pm	0.12337
Off-Peak Summer*	9:30pm-8:30am	0.1177
Part-Peak Winter	8:30am-9:30pm	0.11527
Off-Peak Winter*	9:30pm-8:30am	0.11461
Demand Charges		
Rate	**Period**	**($\$/kW$)**
Peak Summer	12:00pm-6:00 pm	17.26
Part-Peak Summer	8:30am-6:00pm and 6pm-9:30pm	17.26
Maximum Summer*	all time	19.68
Maximum Winter*	all time	19.68

Table 2: PG&E E-20 Transmission Firm. Winter and Summer rates are effective in November-April and May-October, respectively. Rates are in effect during the period times listed for Monday-Friday, excluding holidays. *"Off-peak" and "Maximum" include Saturdays, Sundays, and holidays.

4. RESULTS

In this section, we analyze the results obtained from the digital twin platform for the case study described in Section 3 and compare these with a baseline of historic status-quo operations. First, we evaluate outcomes for a week of optimized operations with full PV solar capacity and battery storage system when using perfect forecasts. Second, we vary the solar capacity and assess the impact of including the storage system. Third, we evaluate the seasonal variance of the platform's performance. Fourth, we assess the impacts of uncertainty in solar generation and grid emissions by integrating simple forecast models and comparing them with achieved results from perfect forecasts.

All optimizations had a seven-day horizon starting at 3 am with $\Delta_t = 0.25$ hours. Using model predictive control, the optimization is run at an alternating frequency of three and four days with two optimizations per week, with the first commencing on Sunday and the second on Wednesday. We saved results from the first three days (Sunday-Wednesday) of the first optimization of each week, then used the SoC of the buses and battery storage at Wednesday 3 am to initialize the second optimization, from which we save the first four days of results (Wednesday-Saturday) to produce a full week of results.

We simulated eight scenarios: three baseline scenarios that evaluate system performance based on historic bus charging and solar generation data collected from meters at the bus depot and five optimized scenarios produced by the platform. The scenarios are notated in this format: *AAA-G+SX+B*. *AAA* can be either *OPT* or *BAS*, which denote an optimization or baseline scenario, respectively. The combinations of *G+S+B* indicate the sources of power available to supply the system: the grid (*G*), the PV solar array (*S*), and the stationary battery storage (*B*). *X* can be *100* or *50*, referring to the percentage of solar capacity for the solar array relative to the actual capacity.

The platform's optimization was solved using Gurobi 10.0.1 with stopping criteria of an absolute objective value gap of $\$50$ and a maximum time limit of 7 hours, except for cases that did not find a solution, which were re-run with a 10-hour limit. For the main *OPT-G+S+B* scenario for the week of March 12, the problem had 80559 continuous decision variables and 57534 binary variables. It was solved in 51.8 minutes on a compute instance with 32 vCPU and 100GB RAM.

4.1 Main Scenario: OPT-G+S+B in March

From the bus data provided by Stanford University, we chose to evaluate the second full week of January, March, and May 2023 to assess seasonal variation across weeks during the academic quarter. We first focus on the results for March, which has solar generation levels in between those of January and May, and compare the baseline scenario *BAS-G+S*, which represents the actual scenario at Stanford University, with the optimized scenario *OPT-G+S+B*, a simulation of platform operations that also includes a battery storage system. We first assume perfect forecasts (i.e., no uncertainty in solar generation and grid emissions) to assess the lower bound on total net cost.

As both baseline and optimized scenarios serve the same routes, they have similar total bus charger energy consumption, 21791 kWh and 19683 kWh, respectively. The small variation is due to differences in bus size assignments, the accuracy of the surrogate model for bus energy consumption, unknown deviations from the nominal bus schedule and starting/ending SoC of buses in the baseline, and losses from charging/discharging the battery storage in the optimized scenario.

Fig. 4 shows a breakdown of the power supplies and demands in the baseline and optimized scenarios. For the baseline scenario, bus drivers simply charge the buses whenever they return to the depot, so there are demand concentrations in the evening when there is no solar generation and power must be drawn from the grid. In comparison, the optimized scenario shifts most of the charging to midday, increasing usage of carbon-free solar power and reducing grid demand. Additionally, charging occurs mostly on weekdays in the baseline in contrast to all days of the week when optimized. Fig. 4 also highlights how battery storage is utilized to reduce emissions. The battery charges only during midday when there is carbon-free solar generation and discharges power to the bus chargers in the evening to recharge the few buses that are in service from morning to evening and cannot charge when solar generation is available.

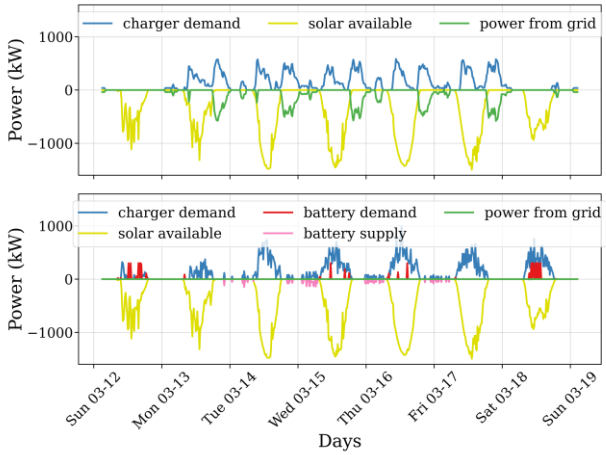

Fig. 4. Breakdown of power demand (bus chargers and battery charging) and power supply (grid, solar, and battery discharging) for the *BAS-G+S* (top) and *OPT-G+S+B* (bottom) scenarios.

Fig. 5 shows the resulting grid power profiles for the two scenarios. Notably, the baseline scenario has grid demand in the evenings, when marginal emissions are highest (see Fig. 3). In contrast, the optimized scenario has nearly zero grid demand, except for a 6kW power draw on Saturday that occurs at a time when the emissions factor is 0 $kg \cdot CO_2/kWh$. As a result, the optimized scenario achieves 24/7 carbon-free operations and reduces emissions by 100% (6.36 tCO_2), peak demand by 99% (574 kW), and total net cost by $3923. In the baseline scenario, the non-optimal solar utilization leads to more surplus power injected back into the grid (i.e., other university facilities), which is accounted for as increased revenue. However, this is offset by increased energy charges due to more use of grid power. Thus, the sum of revenue and energy charges between the baseline and optimized scenarios is similar (-$3576 and -$3755, respectively), which is expected as the charger energy consumption is similar and time-of-use energy rates do not vary significantly over the day. In summary, total net cost reductions are driven by demand charge and emissions cost reductions, not by energy charge and revenue.

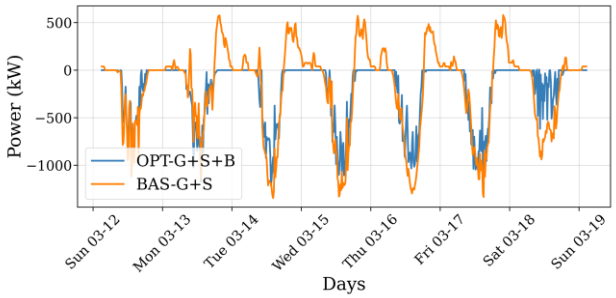

Fig. 5. Grid power in the week of March 12-19 for the *OPT-G+S+B* case (blue) and the *BAS-G+S* (orange).

4.2 Varying solar and battery assumptions

In this subsection, we evaluate cases in which the bus depot solar capacity is 0.9 MW, half of its present capacity, and in which the battery storage system is excluded. Fig. 6 compares grid power profiles for *BAS-G+S50*, *OPT-G+S50*, and *OPT-G+S50+B* with emissions factors overlaid. Similar to the baseline scenario in Section 4.1, *BAS-G+S50* has high grid consumption in the evening that coincides with high grid emissions. In contrast, when *OPT-G+S50* draws grid power, it is typically when emissions are at a local minimum. Similar to the optimized scenario in Section 4.1, the *OPT-G+S50+B* case leverages the battery storage in evenings to recharge those buses that operate from morning to evening, and its remaining grid consumption is limited to midday on days when emissions factors are 0 $kg.CO_2/kWh$, allowing this scenario to achieve 24/7 carbon-free operations.

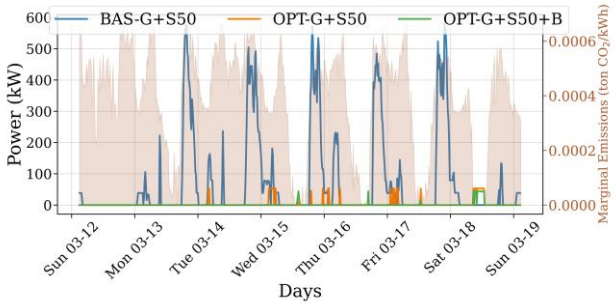

Fig. 6. Power drawn from grid for *BAS-G+S50*, *OPT-G+S50*, and *OPT-G+S50+B* scenarios overlaid with emissions factors for the week of March 12-19. The optimized cases draw grid power at times with lower or no emisissions.

Week	Scenario	Energy Charge ($)	Demand Charge ($)	Revenue ($)	Emission Cost ($)	Emissions (ton)	Power Peak (kW)	Total Net Cost ($)
Jan 8-14	OPT-G+S+B	569	244	0	286	**1.59**	54	**1099**
	OPT-G+S	623	483	8	288	1.6	107	1386
	OPT-G+S50+B	1635	494	0	891	4.95	109	3020
	OPT-G+S50	1636	530	1	860	4.78	117	3025
	OPT-G	2618	748	0	1436	7.98	165	4802
	BAS-G+S	1854	3315	1270	1102	6.12	732	5001
	BAS-G+S50	2034	3315	476	1201	6.67	732	6074
	BAS-G	2532	3315	0	1431	7.95	732	7278
Mar 12-18	OPT-G+S+B	412	26	4167	0	**0.00**	6	**-3729**
	OPT-G+S	400	241	4222	14	0.08	53	-3567
	OPT-G+S50+B	483	199	1100	0	**0.00**	44	-418
	OPT-G+S50	465	241	1070	22	0.12	53	-342
	BAS-G+S	1381	2625	4957	1145	6.36	580	194
	BAS-G+S50	1471	2625	2005	1201	6.67	580	3292
	OPT-G	2433	966	0	1121	6.23	213	4520
	BAS-G	2508	2642	0	1535	8.53	584	6685
May 14-20	OPT-G+S+B	186	36	8369	0	**0.00**	8	**-8147**
	OPT-G+S	279	241	8394	0	**0.00**	53	-7874
	OPT-G+S50+B	251	67	3211	0	**0.00**	15	-2893
	OPT-G+S50	284	241	3192	2	0.01	53	-2665
	BAS-G+S	1407	5547	9230	754	4.19	653	-1522
	BAS-G+S50	1515	5674	4125	815	4.53	668	3879
	OPT-G	2701	1606	0	729	4.05	308	5036
	BAS-G	2603	7924	0	1093	6.07	688	11620

Table 3: Results for all scenarios using perfect forecast. Observe that the Total Net Cost is the sum of the Energy Charge, Demand Charge, and Emissions Cost minus the Revenue (which refers to energy costs that can be offset by power injected back to the grid).

4.3 *Comparison of seasonal performance*

As solar generation, marginal grid emissions factors, bus energy consumption, and electric utility rates vary by time of year, we performed case studies for fleet operations in January, March, and May to evaluate the 24/7 CFEF platform's performance across seasons. Table 3 reflects the results obtained for the second full week of January, March, and May, assuming a perfect forecast and ordered from lowest to highest total net cost. Figs. 7 and 8 show emissions and cost reductions, respectively, for each optimization scenario and its corresponding baseline. Taking advantage of the greater solar generation in March and May allows the platform to further reduce emissions reductions compared to the baseline. Integrating a stationary battery enables a 24/7 decarbonized system in March, even with only moderate solar generation. In January, however, when solar generation is low, the case with the battery has slightly increased emissions. This occurs because the optimization is minimizing the total net cost, so the battery dispatch prioritizes decreasing demand charges, the most significant cost term, over emissions reduction. When solar generation is abundant in May, a 24/7 decarbonized system is possible with and without the battery. However, integrating the battery further reduces total net cost.

4.4 Dealing with uncertainty

We conclude our analysis by assessing the platform's performance under uncertainty of marginal grid emissions factors and solar generation compared to its lower bound results obtained with perfect forecasts. Fig. 9 presents the accuracy of the surrogate model (top) and performance of simple forecasters (bottom) described in Section 2. Recall that for the surrogate model, the prior 30 days were used as training data while the next seven days' features and energy consumption were used to validate the model. The model has an R^2 value between 0.84 and 0.94 and MSE lower than 0.004. For the forecasts, the solar and weather forecast errors were larger for January and March due to cloudy and rainy days. Performance improved in May with more consistent weather (i.e., constant sun).

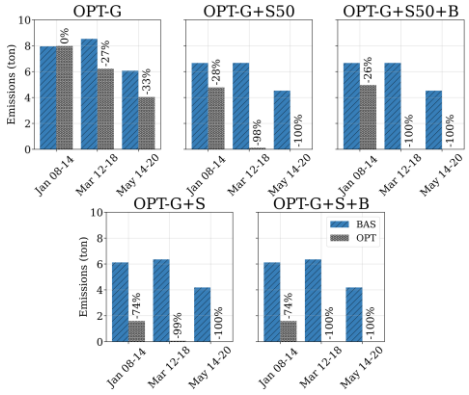

Fig. 7. Comparison of emissions between each optimization scenario and their corresponding baseline.

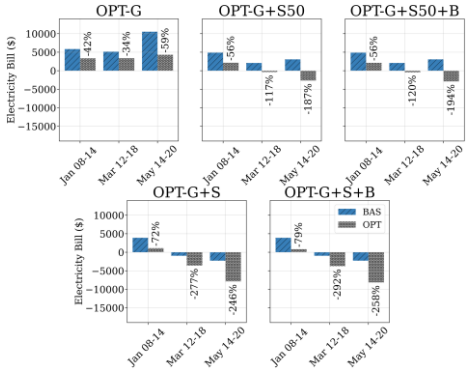

Fig. 8. Comparison of electricity bill between each optimization scenario and their corresponding baseline.

Given the performance of solar generation forecasts, we investigated how adding a buffer to the solar forecast could improve overall results. In general, when the solar forecast underpredicts, the chargers and battery use surplus solar generation if they have unmet demand, and any remaining surplus is injected into the grid. When the forecast overpredicts, solar generation is distributed to the chargers and battery, and the grid fulfils the remaining demand. The buffer serves to reduce instances of overprediction, which often leads to expensive demand charges and carbon-emitting grid usage. The results of the platform when using buffered solar forecasts, which reduces the forecasted solar by a

constant factor, are shown in Table 4. We assess three uncertainty cases, *OPT-G+S+B-forecast-S100*, *OPT-G+S+B-forecast-S80*, and *OPT-G+S+B-forecast-S50*, wherein the weather and emissions forecasts are unchanged, and the solar forecast is multiplied by 100%, 80%, and 50%, respectively. We then evaluate the optimized actions using the actual solar and emissions profiles. In all the cases, optimization scenarios with uncertainty still outperform the baseline in total net cost and emissions. Among the uncertainty cases, the most conservative buffer (*OPT-G+S+B-forecast-S50*) reduces the electricity bill relative to the baseline the most due to lower demand charges.

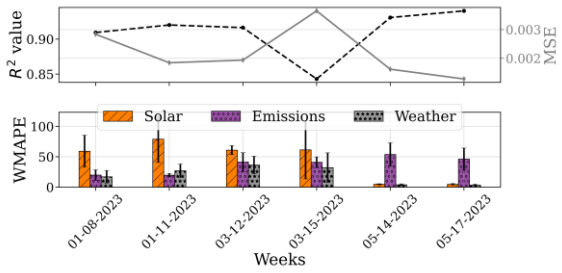

Fig. 9. Surrogate model evaluation for test samples based on the R^2 and MSE metrics for each optimization (top) and *WMAPE* values for solar, emissions, and weather forecasts (bottom). The bars show the average *WMAPE* of the seven-day forecasts beginning on the indicated date, and the error bars show the standard deviation.

While the optimization platform shows significant cost and emissions reductions compared to the baseline even when using naive forecasts, numerous strategies could be employed to improve its performance under uncertainty and close the gap with the lower bound of perfect forecast. Besides the buffer approach, other methods include (i) more frequent evaluations (e.g., daily) of the platform to have more updated forecasts, (ii) employing stochastic optimization in the platform's optimization module, (iii) incorporating more sophisticated forecast models such as attention-based mechanisms coupled with other covariates like weather features, and (iv) introducing a real-time controller for the stationary battery that will discharge the battery in response to demand spikes.

5. CONCLUSIONS

In this work, we developed a digital twin framework to coordinate electric bus fleet charging and bus assignments. We accounted for stationary battery storage charging/discharging, PV solar generation, and marginal grid emissions. Results demonstrated that the proposed method reduced emissions by roughly 74% during a winter week and achieved 24/7 carbon-free operations during spring weeks with a perfect forecast. Total net cost was reduced by approximately $3901 in winter and at least $3923 in spring. Moreover, using simple naive forecast models for marginal emissions and solar generation, the platform reduced up to 43% of carbon emissions during a winter week, depending on the buffer strategy, and at least 63% during spring. Total net cost was reduced by up to $1773 in winter and at least $1504 in spring.

This success in cost-effective emissions reduction opens several avenues for future work. An immediate next step is to optimize solar array and stationary battery sizing to achieve 24/7 carbon-free operations in all weeks of the year. Additionally, we will validate simulated results by deploying the digital twin platform in a pilot with the Stanford Marguerite Shuttle. Further, a sensitivity analysis of emissions concerning the price of carbon can advise carbon pricing policy for 24/7 carbon-free transportation. Next, the methodologies discussed in Section 4.4 can be investigated to improve the platform's robustness to uncertainty. Finally, we can employ the digital twin framework to enable 24/7 carbon-free operations in other applications, such as electric fleets used by school districts, public transportation, corporate campuses, delivery services, autonomous shuttles, airports, and municipalities.

Week	Scenario	Electricity Bill ($)	(%)	Emissions (ton)	(%)	Total Net Cost ($)	(%)
Jan 8-14	BAS-G+S	3899	-	6.12	-	5001	-
	OPT-G+S+B	813	-79	1.59	-74	1100	-78
	OPT-G+S+B-forecast-S100	3301	-15	3.48	**-43**	3927	-21
	OPT-G+S+B-forecast-S80	3122	-20	3.93	-36	3829	-23
	OPT-G+S+B-forecast-S50	2258	**-42**	5.39	-12	3228	**-35**
Mar 12-18	BAS-G+S	-951	-	6.36	-	193	-
	OPT-G+S+B	-3730	-292	0.00	-100	-3730	-2031
	OPT-G+S+B-forecast-S100	-393	59	0.61	**-90**	-283	-246
	OPT-G+S+B-forecast-S80	-701	26	1.19	-81	-488	-353
	OPT-G+S+B-forecast-S50	-1735	**-82**	2.36	-63	-1311	**-779**
May 14-20	BAS-G+S	-2276	-	4.19	-	-1522	-
	OPT-G+S+B	-8146	-258	0.00	-100	-8146	-435
	OPT-G+S+B-forecast-S100	-7727	-239	0.29	-93	-7675	-404
	OPT-G+S+B-forecast-S80	-7481	-229	0.19	**-96**	-7448	-389
	OPT-G+S+B-forecast-S50	-8140	**-258**	0.15	**-96**	-8113	**-433**

Table 4: Results for *BAS-G+S* and *OPT-G+S+B* compared to scenarios with uncertainty with varying buffer levels in solar generation forecast. Absolute and relative results for the electricity bill, emissions, and total net cost are shown.

ACKNOWLEDGEMENT

This publication was supported by the Fulbright U.S. Student Program, CAPES – Brazil (Finance Code 001), the Stanford University Bits & Watts Initiative, and the Stanford Sustainability Accelerator. The views expressed are those of the authors and do not necessarily reflect the official policy of the Fulbright Program, the U.S. Government, CAPES/Brazil, or Stanford University. We thank the Stanford Research Computing Center for computational resources and support on the Sherlock cluster, which aided this research.

DECLARATION OF INTEREST STATEMENT

The authors declare that they have no known competing financial interests or personal relationships that could have appeared to influence the work reported in this paper. All authors read and approved the final manuscript.

REFERENCE

[1] Energy Information Administration. *U.S. energy facts explained - consumption and production* - U.S. Energy Information Administration (EIA). 2022.

[2] United Nations. *Causes and Effects of Climate Change*. en. Publisher: United Nations. 2023.

[3] S. Powell et al. "Charging infrastructure access and operation to reduce the grid impacts of deep electric vehicle adoption". en. In: *Nature Energy* 7.10 (Oct. 2022). Number: 10 Publisher: Nature Publishing Group, pp. 932–945. DOI: 10.1038/s41560-022-01105-7.

[4] California Air Resources Board. *Innovative Clean Transit (ICT) Regulation*. 2019.

[5] W. H. Green et al. "Insights Into Future Mobility: A Report from the Mobility of the Future Study". In: (Nov. 2019).

[6] A. Rong et al. "A Review on Electric Bus Charging Scheduling from Viewpoints of Vehicle Scheduling". In: *2021 IEEE International Conference on Industrial Engineering and Engineering Management (IEEM)*. Dec. 2021, pp. 1–5. DOI: 10.1109/IEEM50564.2021.9673069.

[7] S. S. G. Perumal, R. M. Lusby, and J. Larsen. "Electric bus planning & scheduling: A review of related problems and methodologies". en. In: *European Journal of Operational Research* 301.2 (Sept. 2022), pp. 395–413. DOI: 10. 1016/j.ejor.2021.10.058.

[8] J. Shu, S. Chen, and Z. Ding. "Locational Price Driven Electric Bus Fleet Operation and Charging Demand Management". In: *2021 IEEE/IAS Industrial and Commercial Power System Asia (I&CPS Asia)*. July 2021, pp. 409–413. DOI: 10.1109/ICPSAsia52756.2021.9621397.

[9] A. Kunith, R. Mendelevitch, and D. Goehlich. "Electrification of a city bus network—An optimization model for cost-effective placing of charging infrastructure and battery sizing of fast-charging electric bus systems". In: *International Journal of Sustainable Transportation* 11.10 (Nov. 2017). Publisher: Taylor & Francis pp. 707– 720. DOI: 10.1080/15568318.2017.1310962.

[10] Y. Wang et al. "Optimal recharging scheduling for urban electric buses: A case study in Davis". en. In: *Transportation Research Part E: Logistics and Transportation Review* 100 (Apr. 2017), pp. 115–132. DOI: 10.1016/j.tre. 2017.01.001.

[11] L. Li, H. K. Lo, and F. Xiao. "Mixed bus fleet scheduling under range and refueling constraints". en. In: *Transportation Research Part C: Emerging Technologies* 104 (July 2019), pp. 443–462. DOI: 10.1016/ j.trc.2019.05.009.

[12] O. Battaïa et al. "MILP model for fleet and charging infrastructure decisions for fast-charging city electric bus services". en. In: *Computers & Industrial Engineering* 182 (Aug. 2023), p. 109336. ISSN: 0360-8352. DOI: 10.1016/j.cie.2023.109336.

[13] N. Guschinsky et al. "Fleet and charging infrastructure decisions for fast-charging city electric bus service". en. In: *Computers & Operations Research* 135 (Nov. 2021), p. 105449. DOI: 10.1016/j.cor.2021.105449.

[14] G. Wang et al. "bCharge: Data-Driven Real-Time Charging Scheduling for Large-Scale Electric Bus Fleets". In: *2018 IEEE Real-Time Systems Symposium (RTSS)*. Dec. 2018, pp. 45–55. DOI: 10.1109/RTSS.2018.00015.

[15] A. Houbbadi et al. "Optimal Charging Strategy to Minimize Electricity Cost and Prolong Battery Life of Electric Bus Fleet". In: *2019 IEEE Vehicle Power and Propulsion Conference (VPPC).* ISSN: 1938-8756. Oct. 2019, pp. 1–6. DOI: 10.1109/VPPC46532.2019.8952493.

[16] A. Moradipari et al. "Mobility-Aware Smart Charging of Electric Bus Fleets". In: *2020 IEEE Power & Energy Society General Meeting (PESGM)*. ISSN: 1944-9933. Aug. 2020, pp. 1–5. DOI: 10.1109/PESGM41954.2020.9281897.

[17] K.-W. Cheng et al. *Carbon-Aware EV Charging*. arXiv:2209.12373 [cs,eess]. Sept. 2022. DOI: 10.48550/arXiv.2209.12373.

[18] R. Tu et al. "Electric vehicle charging optimization to minimize marginal greenhouse gas emissions from power generation". In: *Applied Energy* 277 (Nov. 2020), p. 115517. DOI: 10.1016/j.apenergy.2020.115517.

[19] C. E. Rasmussen and C. K. I. Williams. *Gaussian processes for machine learning*. en. Adaptive computation and machine learning. OCLC: ocm61285753. Cambridge, Mass: MIT Press, 2006. ISBN: 978-0-262-18253-9.

[20] M. J. Kochenderfer, T. A. Wheeler, and K. H. Wray. *Algorithms for decision making*. en. Cambridge, Massachusetts: The MIT Press, 2022. ISBN: 978-0-262-04701-2.

[21] K. Ricke et al. "Country-level social cost of carbon". en. In: *Nature Climate Change* 8.10 (Oct. 2018). Number: 10 Publisher: Nature Publishing Group, pp. 895–900. DOI: 10.1038/s41558-018-0282-y.